

Electronic Supplementary Information

Computational, Electrochemical, and Spectroscopic Studies of two Mononuclear Cobaloximes: The influence of an axial pyridine and solvent on the redox behaviour and evidence for pyridine coordination to cobalt(I) and cobalt(II) metal centres.

Mark A. W. Lawrence,^a Michael J. Celestine,^a Edward T. Artis,^a Lorne S. Joseph,^b Deisy L. Esquivel,^c Abram J. Ledbetter,^d Donald M. Cropek,^e William L. Jarrett,^f Craig A. Bayse,^a Matthew I. Brewer,^a and Alvin A. Holder*^a

Table of Contents

| | |
|--|----|
| Electronic Supplementary Information | 1 |
| 1 Results | 2 |
| 1.1 Characterization | 2 |
| 1.2 Mole ratio plots and equilibria data | 5 |
| 1.3 Electrochemical data | 16 |
| 1.4 Spectroelectrochemical data | 22 |
| 1.5 ^{11}B , ^{19}F , and ^{59}Co NMR spectroscopic data..... | 31 |
| 1.6 Electrocatalytic behaviour..... | 34 |

1 Results

1.1 Characterization

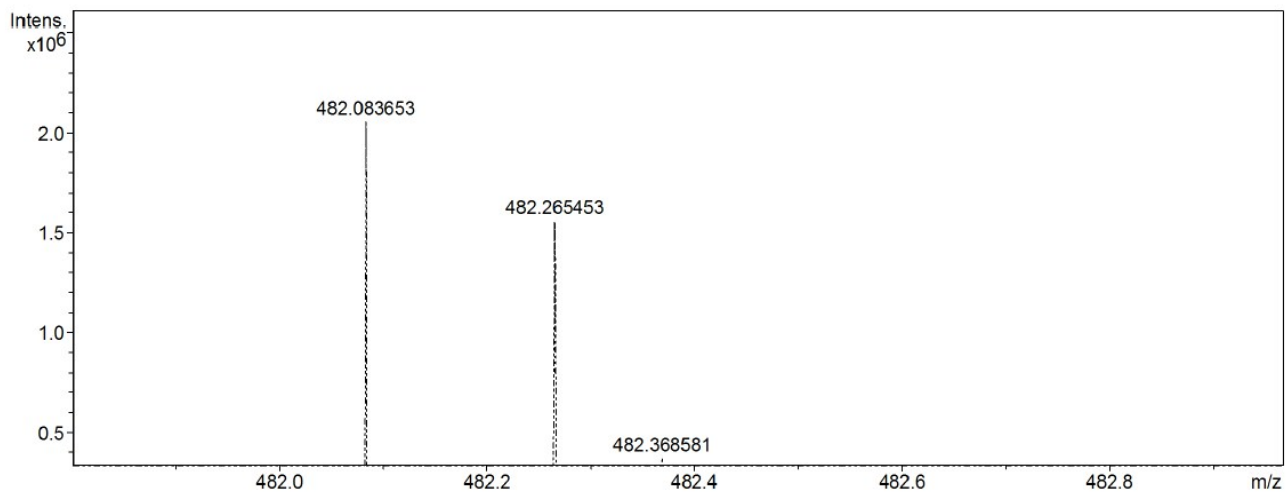
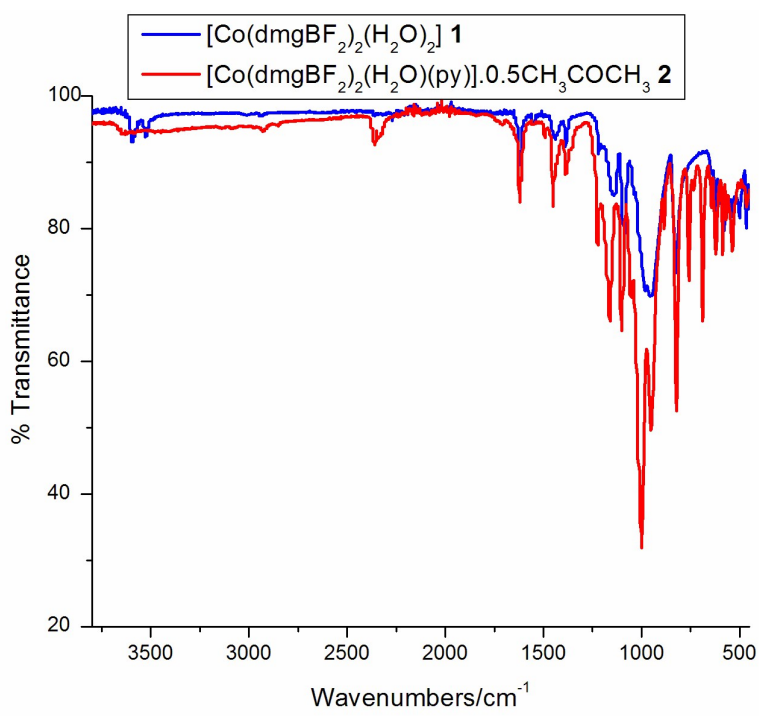


Figure S1. High resolution ESI mass spectrum of $[\text{Co}(\text{dmgBF}_2)_2(\text{H}_2\text{O})(\text{py})]^+$ in the positive mode with CH_3CN as solvent.



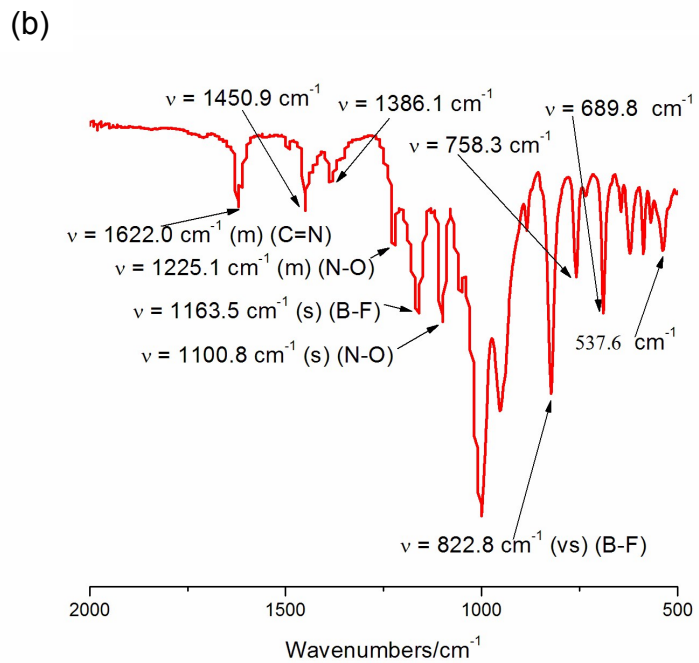
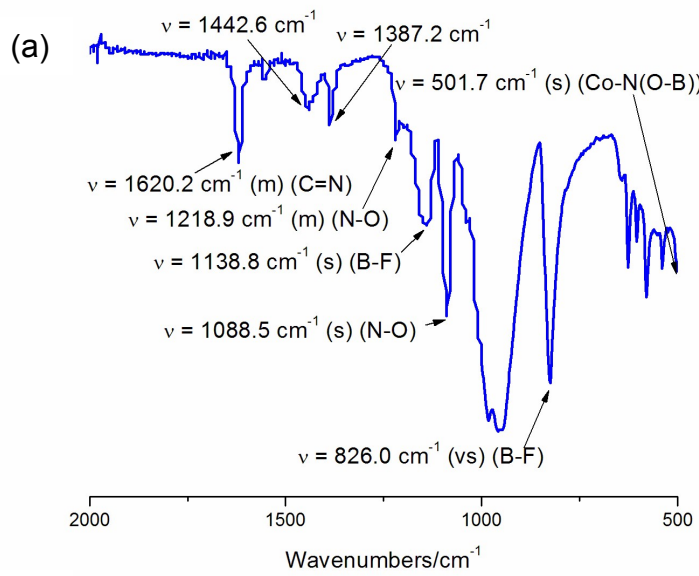


Figure S2. Full FT IR spectra and assignment of selected stretching frequencies of (a) complex **1** and (b) complex **2**.

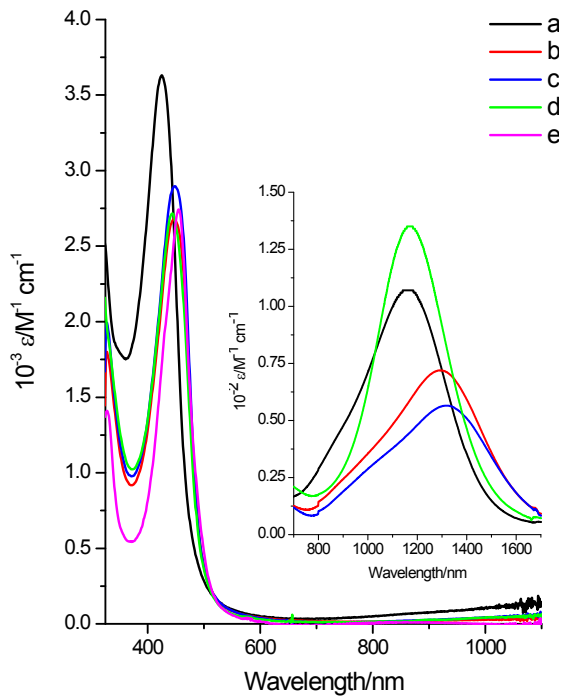


Figure S3. A plot of the molar extinction coefficient versus wavelength of complex **1**. Solvent = acetonitrile (a), acetone (b), 2-butanone (c), 1,2-difluorobenzene/acetone (4:1, v/v) (d), and water (e). NIR spectrum is shown as an inset.

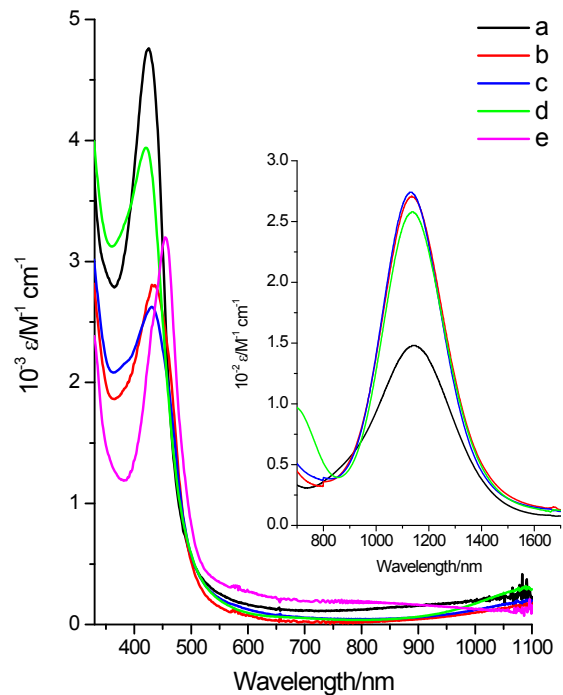


Figure S4. A plot of the molar extinction coefficient versus wavelength of complex **2**. Solvent = acetonitrile (a), acetone (b), 2-butanone (c), 1,2-difluorobenzene/acetone (4:1, v/v) (d), and water (e). NIR spectrum is shown as an inset.

1.2 Mole ratio plots and equilibria studies

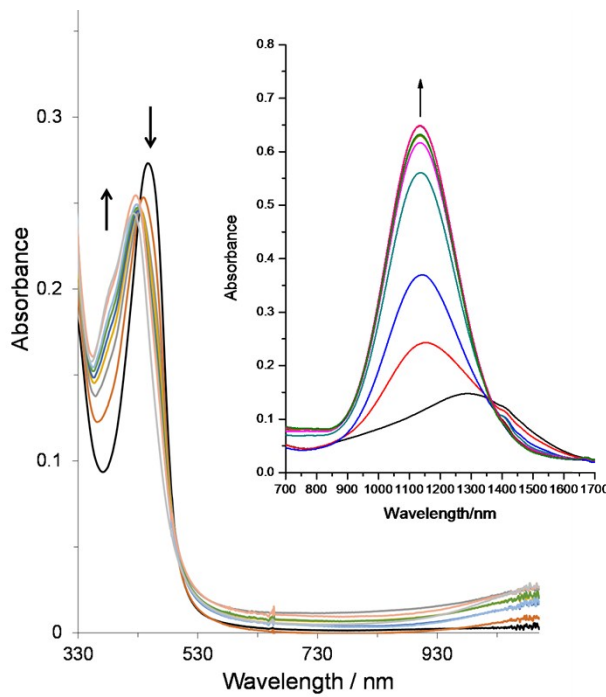


Figure S5. The effect of pyridine addition to complex **1** in the UV-visible spectrum (NIR spectrum is shown as an inset) in acetone. [complex **1**] = 0.1 mM (2.0 mM for NIR spectral studies) and 0.0 mM \geq [pyridine] \geq 0.5 mM (0.0 mM \geq [pyridine] \geq 4.0 mM for NIR spectral studies), and path length = 1.0 cm.

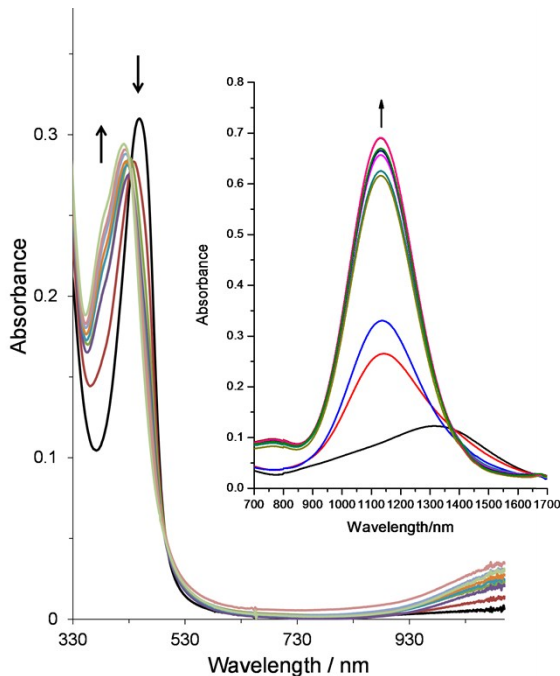


Figure S6. The effect of pyridine addition to complex **1** in the UV-visible spectrum (NIR spectrum is shown as an inset) in 2-butanone. [complex **1**] = 0.1 mM (2.0 mM for NIR spectral studies) and 0.0 mM \geq [pyridine] \geq 0.5 mM (0.0 mM \geq [pyridine] \geq 4.0 mM for NIR spectral studies), and path length = 1.0 cm.

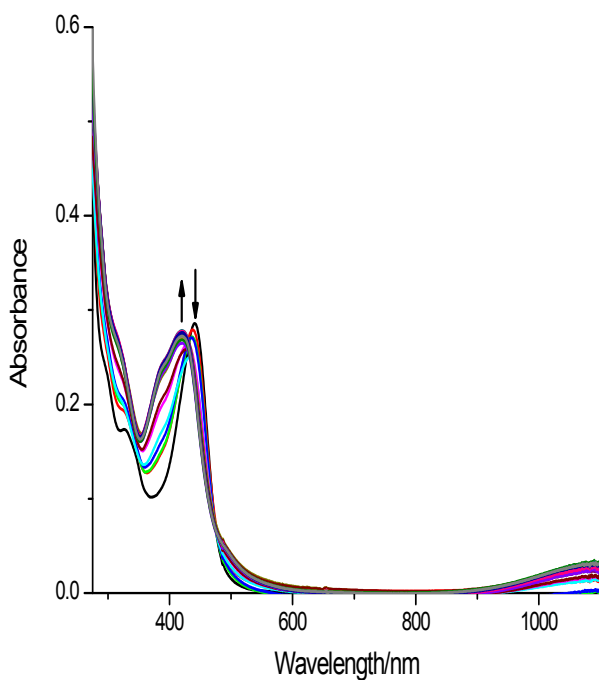


Figure S7. A plot of absorbance versus wavelength for a titration of complex **1** with pyridine in dichloromethane at 20 °C. [Complex **1**] = 0.10 mM and path length = 1.0 cm.

Table S1. NIR spectral data for absorbance at 1162 nm, $\log [(A_o - A)/(A - A_\infty)]$, and $\log [\text{pyridine}]$ for complex **1** in acetonitrile at 20 °C. [complex **1**] = 2.0 mM and path length = 1.0 cm.

| [py]/[complex 1] | Abs _{1162 nm} | $\log [\text{pyridine}]$ | $\log [(A_o - A)/(A - A_\infty)]$ |
|--------------------------|------------------------|--------------------------|-----------------------------------|
| 0 | 0.2474 | -- | --- |
| 0.25 | 0.2892 | -3.572 | -0.8823 |
| 0.33 | 0.3059 | -3.474 | -0.7130 |
| 0.40 | 0.3222 | -3.414 | -0.5821 |
| 0.50 | 0.3344 | -3.286 | -0.4977 |
| 0.65 | 0.36315 | -3.182 | -0.3254 |
| 0.75 | 0.3720 | -3.092 | -0.2774 |
| 0.87 | 0.3895 | -3.021 | -0.1870 |
| 1.0 | 0.4062 | -2.951 | -0.1040 |
| 1.12 | 0.4255 | -2.902 | -0.0107 |
| 1.50 | 0.4645 | -2.746 | 0.1800 |
| 1.75 | 0.4845 | -2.661 | 0.2831 |
| 2.0 | 0.4949 | -2.580 | 0.3401 |
| 2.25 | 0.5103 | -2.517 | 0.4301 |
| 2.75 | 0.5131 | -2.395 | 0.4473 |
| 3.0 | 0.5258 | -2.351 | 0.5295 |
| 4.0 | 0.5495 | -2.199 | 0.7126 |
| 5.0 | 0.5562 | -2.082 | 0.7756 |

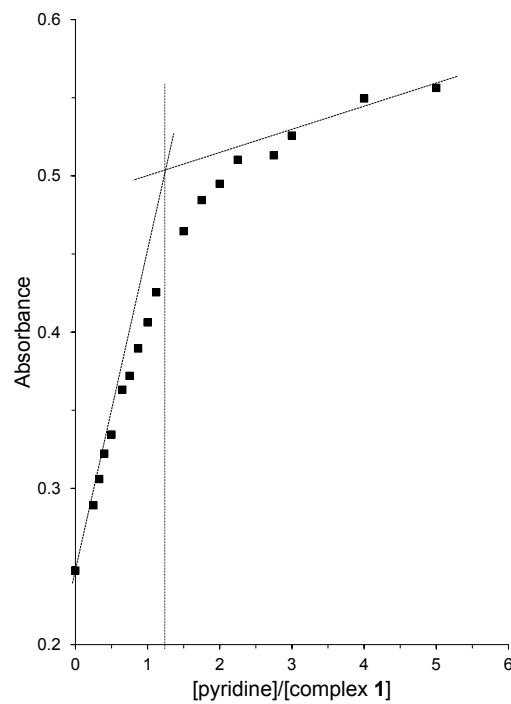


Figure S8. Mole ratio plot for the interaction of pyridine with complex **1** in acetonitrile. [complex **1**] = 2.0 mM, λ = 1162 nm, temperature = 20 °C, and path length = 1.0 cm.

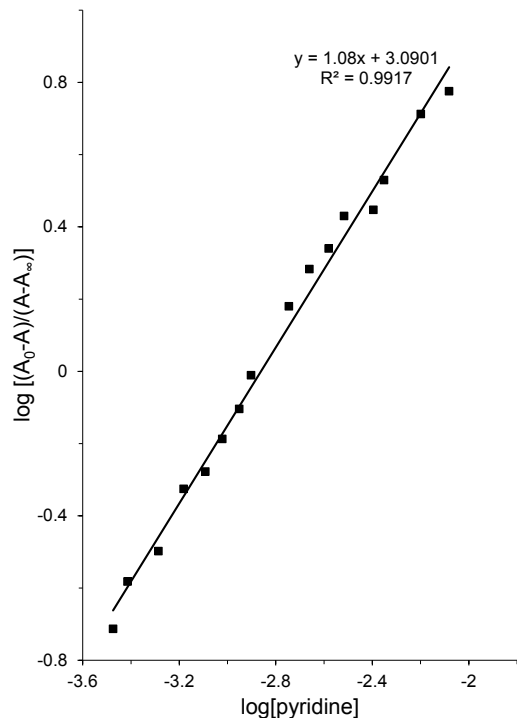


Figure S9. A plot of $\log [(A_0 - A)/(A - A_\infty)]$ versus $\log [\text{pyridine}]$ for complex **1** at 1162 nm in acetonitrile at 20 °C.

Table S2. UV-visible spectral data for absorbance at 372 nm, $\log [(A_o - A)/(A - A_\infty)]$, and $\log [\text{pyridine}]$ for complex **1** in acetone at 20 °C. [complex **1**] = 0.10 mM and path length = 1.0 cm.

| [py]/[complex 1] | Abs _{372 nm} | $\log [(A_o - A)/(A - A_\infty)]$ | $\log [\text{pyridine}]$ |
|--------------------------|-----------------------|-----------------------------------|--------------------------|
| 0 | 0.0922 | --- | --- |
| 0.50 | 0.1265 | -0.2309 | -4.886 |
| 0.87 | 0.1444 | 0.1099 | -4.513 |
| 1.0 | 0.1497 | 0.2128 | -4.420 |
| 1.25 | 0.1590 | 0.4103 | -4.276 |
| 1.50 | 0.1618 | 0.4763 | -4.125 |
| 1.75 | 0.1696 | 0.7018 | -4.038 |
| 2.0 | 0.1724 | 0.8020 | -3.945 |
| 4.0 | 0.1796 | 1.206 | -3.514 |

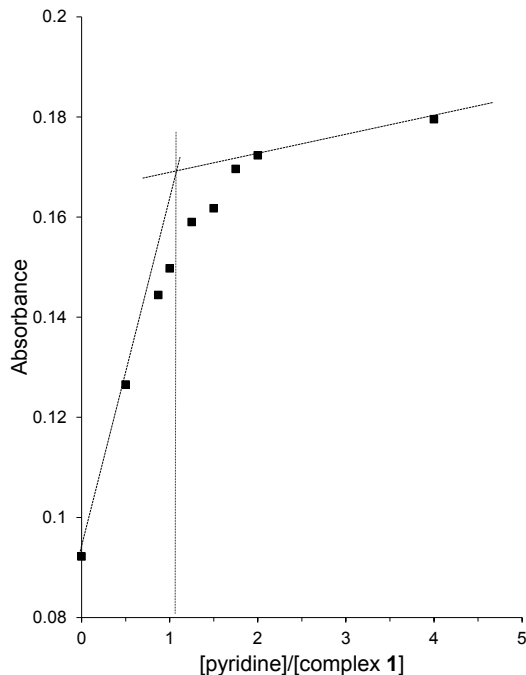


Figure S10. Mole ratio plot for the interaction of pyridine with complex **1** in acetone. [complex **1**] = 0.10 mM, λ = 372 nm, temperature = 20 °C, and path length = 1.0 cm.

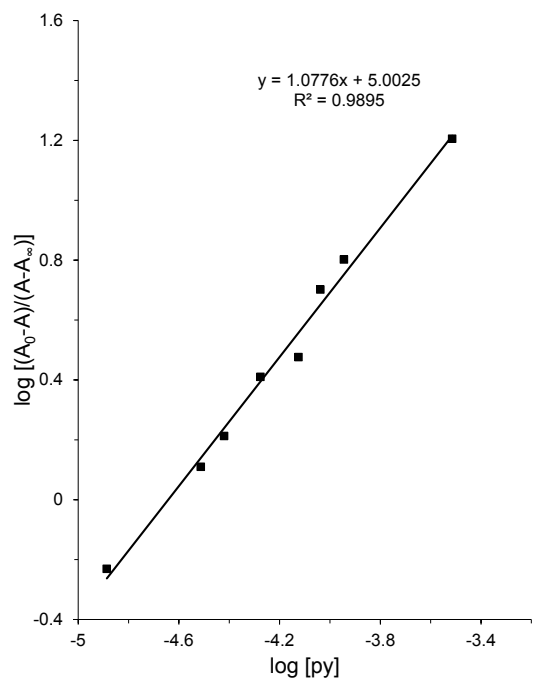


Figure S11. A plot of $\log [(A_0 - A)/(A - A_\infty)]$ versus $\log [\text{pyridine}]$ for complex **1** at 371 nm in acetone at 20 °C.

Table S3. UV-visible spectral data for absorbance at 372 nm, $\log [(A_0 - A)/(A - A_\infty)]$, and $\log [\text{pyridine}]$ for complex **1** in 2-butanone at 20 °C. [complex **1**] = 0.10 mM, and path length = 1.0 cm.

| [py]/[complex 1] | Abs _{372 nm} | $\log [(A_0 - A)/(A - A_\infty)]$ | $\log [\text{pyridine}]$ |
|--------------------------|-----------------------|-----------------------------------|--------------------------|
| 0 | 0.1045 | --- | --- |
| 0.50 | 0.1498 | -4.857 | -0.2480 |
| 1.0 | 0.1847 | -4.442 | 0.2479 |
| 1.25 | 0.1973 | -4.292 | 0.4529 |
| 1.50 | 0.2035 | -4.148 | 0.5716 |
| 1.75 | 0.2105 | -4.043 | 0.7357 |
| 2.0 | 0.2150 | -3.951 | 0.8664 |
| 4.0 | 0.2244 | -3.516 | 1.330 |

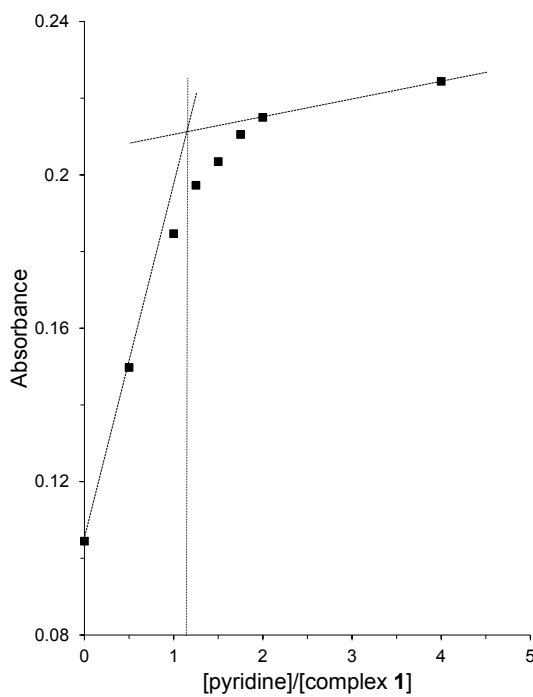


Figure S12. Mole ratio plot for the interaction of pyridine with complex **1** in 2-butanone. [complex **1**] = 0.10 mM, λ = 372 nm, temperature = 20 °C, path length = 1.0 cm.

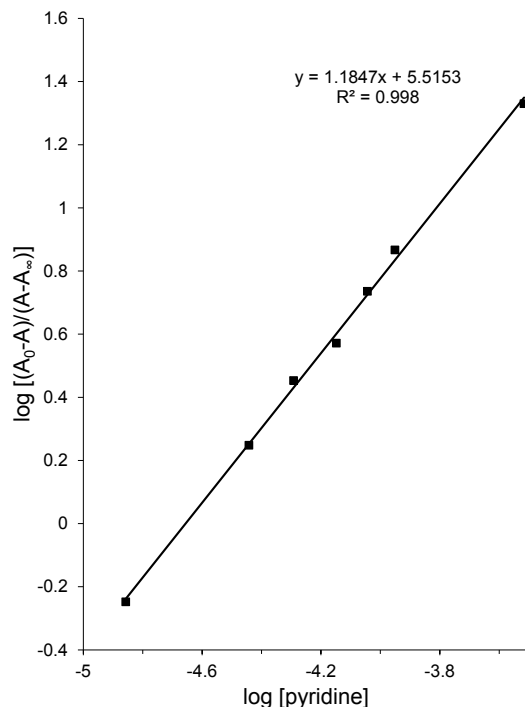


Figure S13. A plot of $\log \left[\frac{(A_0 - A)}{(A - A_\infty)} \right]$ versus $\log [\text{pyridine}]$ for complex **1** at 372 nm in 2-butanone at 20 °C.

Table S4. UV-visible spectral data for absorbance at 372 nm, $\log [(A_o - A)/(A - A_\infty)]$, and $\log [\text{pyridine}]$ for complex **1** in 1,2-difluorobenzene/acetone (4:1, v/v) at 20 °C. [complex **1**] = 0.10 mM, and path length = 1.0 cm.

| [py]/[complex 1] | Abs _{372 nm} | $\log [\text{pyridine}]$ | $\log [(A_o - A)/(A - A_\infty)]$ |
|------------------|-----------------------|--------------------------|-----------------------------------|
| 0 | 0.1058 | --- | --- |
| 0.33 | 0.1336 | -5.349 | -0.3990 |
| 0.40 | 0.1390 | -5.231 | -0.2858 |
| 0.50 | 0.1444 | -4.988 | -0.1810 |
| 0.65 | 0.1556 | -4.860 | 0.02092 |
| 0.75 | 0.1593 | -4.700 | 0.08827 |
| 1.25 | 0.1817 | -4.329 | 0.5519 |
| 1.50 | 0.1864 | -4.173 | 0.6848 |
| 1.75 | 0.1874 | -4.041 | 0.7184 |
| 2.5 | 0.1930 | -3.795 | 0.9394 |
| 5.0 | 0.2011 | -3.396 | 1.7048 |

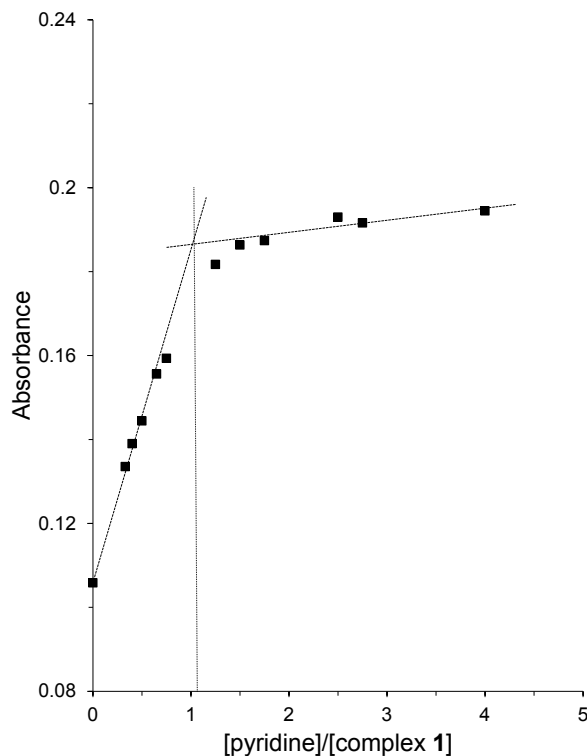


Figure S14. Mole ratio plot for the interaction of pyridine with complex **1** in 1,2-difluorobenzene/acetone (4:1, v/v). [complex **1**] = 0.10 mM, $\lambda = 372$ nm, temperature = 20 °C, path length = 1.0 cm.

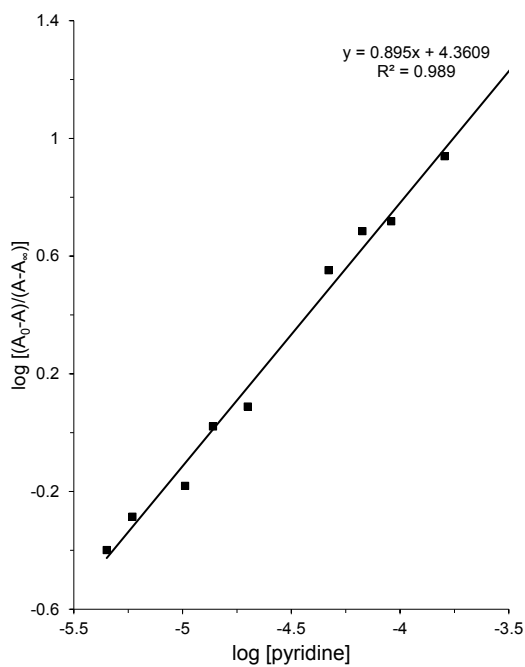


Figure S15. A plot of $\log \left[\frac{(A_0 - A)}{(A - A_\infty)} \right]$ versus $\log [\text{pyridine}]$ for complex **1** at 372 nm in 1,2-difluorobenzene/acetone (4:1, v/v) at 20 °C.

Table S5. UV-visible spectral data for absorbance at 370 nm, $\log \left[\frac{(A_0 - A)}{(A - A_\infty)} \right]$ and $\log [\text{pyridine}]$ for complex **1** in dichloromethane at 20 °C. [complex **1**] = 0.10 mM, and path length = 1.0 cm.

| [py]/[complex 1] | Abs _{370 nm} | $\log [\text{pyridine}]$ | $\log \left[\frac{(A_0 - A)}{(A - A_\infty)} \right]$ |
|--------------------------|-----------------------|--------------------------|--|
| 0 | 0.1016 | -- | -- |
| 0.33 | 0.1341 | -6.166 | -0.3210 |
| 0.40 | 0.1409 | -6.068 | -0.1916 |
| 0.50 | 0.1506 | -5.909 | -0.02143 |
| 0.75 | 0.1738 | -5.507 | 0.4077 |
| 0.87 | 0.1843 | -5.330 | 0.6680 |
| 1.0 | 0.1914 | -4.977 | 0.9282 |
| 1.12 | 0.1949 | -4.720 | 1.121 |
| 1.25 | 0.1964 | -4.514 | 1.226 |
| 1.5 | 0.1977 | -4.265 | 1.350 |
| 2.0 | 0.2003 | -3.993 | 1.755 |
| 2.25 | 0.1997 | -3.895 | 1.635 |
| 2.5 | 0.1991 | -3.816 | 1.531 |
| 3.0 | 0.2011 | -3.697 | 2.025 |

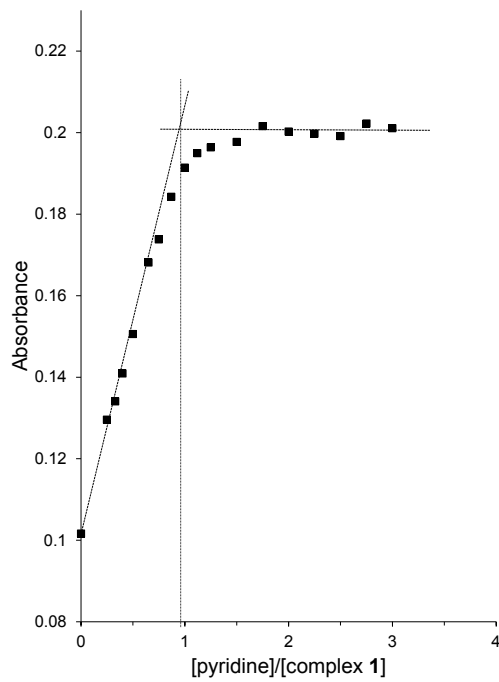


Figure S16. Mole ratio plot for the interaction of pyridine with complex **1** in dichloromethane. [complex **1**] = 0.10 mM, λ = 370 nm, temperature = 20 °C, and path length = 1.0 cm.

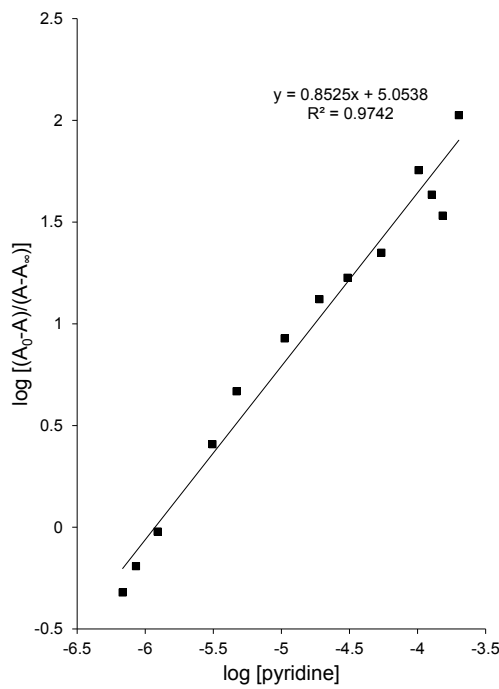


Figure S17. A plot of $\log [(A_0 - A)/(A - A_\infty)]$ versus $\log [\text{pyridine}]$ for complex **1** at 370 nm in dichloromethane at 20 °C.

Table S6. UV-visible spectral data for absorbance at 447 nm, $\log [(A_o - A)/(A - A_\infty)]$, $\log [\text{pyridine}]$ for the $[^n\text{Bu}_4\text{N}]\text{BH}_4$ reduced form of complex **1** in acetonitrile. [complex **1**] = 1.0 mM, temperature = 20 °C, and path length = 1.0 mm.

| [py]/[complex 1] | Abs _{447 nm} | $\log [(A_o - A)/(A - A_\infty)]$ | $\log [\text{py}]$ |
|--------------------------|-----------------------|-----------------------------------|--------------------|
| 0 | 0.1781 | --- | --- |
| 0.5 | 0.2404 | -0.3440 | -3.725 |
| 1.0 | 0.2954 | 0.1524 | -3.384 |
| 1.5 | 0.3199 | 0.3871 | -3.102 |
| 2.0 | 0.3433 | 0.6780 | -2.931 |
| 2.5 | 0.3538 | 0.8610 | -2.790 |
| 4.0 | 0.3689 | 1.322 | -2.516 |

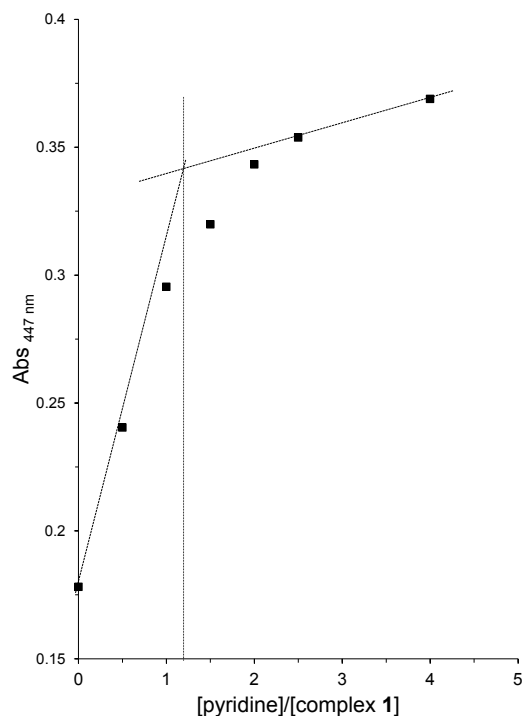


Figure S18. Mole ratio plot for the interaction of pyridine with the $[^n\text{Bu}_4\text{N}]\text{BH}_4$ reduced form of complex **1** in acetonitrile. [complex **1**] = 1.0 mM, temperature = 20 °C, and path length = 1.0 mm.

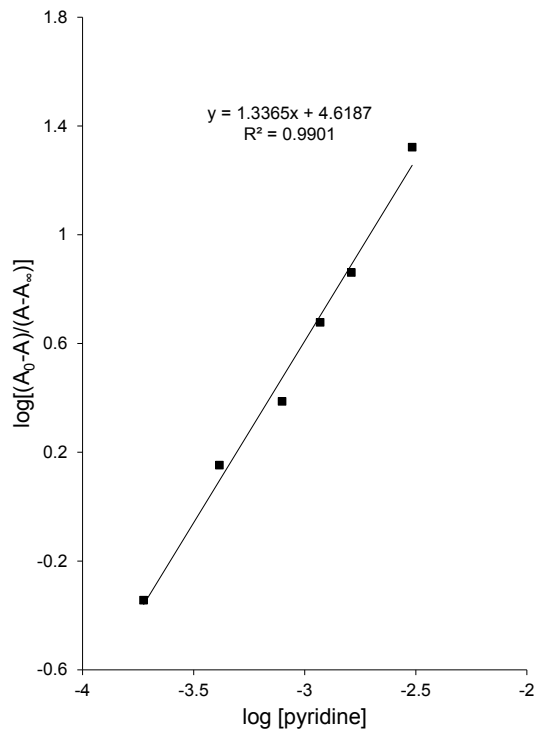


Figure S19. A plot of $\log [(A_0 - A)/(A - A_\infty)]$ versus $\log [\text{py}]$ for the $[n\text{Bu}_4\text{N}]\text{BH}_4$ reduced form of complex **1** in acetonitrile at 20°C .

1.3 Electrochemical data

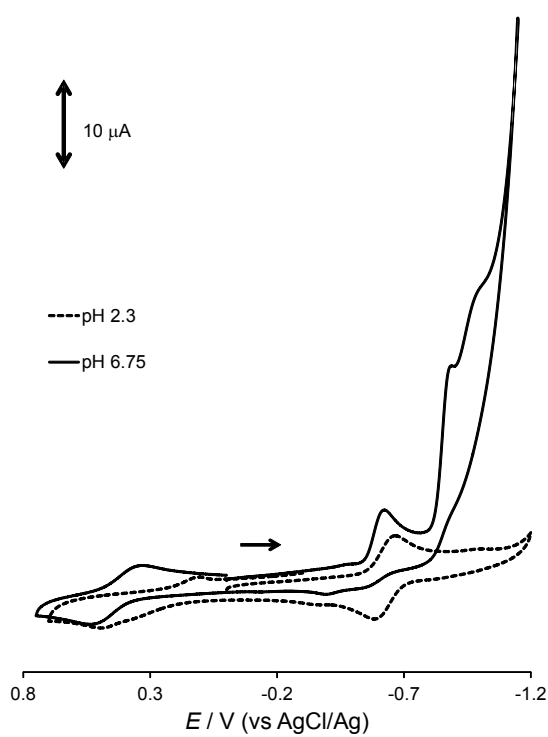


Figure S20. Cyclic voltammograms of complex **1** in water on a glassy carbon working electrode versus AgCl/Ag. [complex **1**] = 0.64 mM, pH = 2.30 (solid lines) and pH = 6.75 (broken lines), supporting electrolyte = 0.10 M NaClO₄, and scan rate = 100 mV s⁻¹.

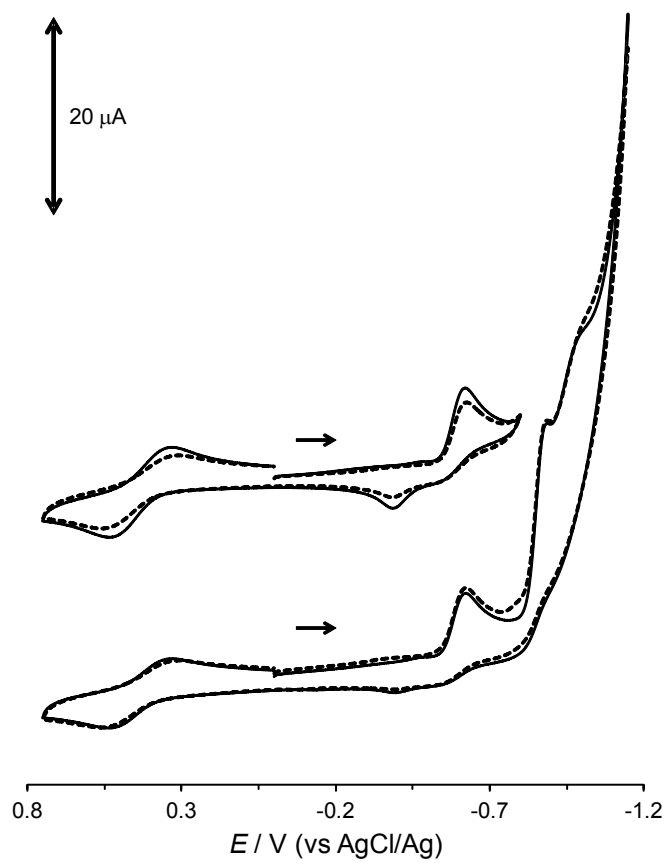


Figure S21. Cyclic voltammograms of complexes **1** and **2** in water on a glassy carbon working electrode versus AgCl/Ag. [complex **1**] = 0.64 mM (solid lines) and [complex **2**] = 0.63 mM (broken lines), pH = 2.30, supporting electrolyte = 0.10 M NaClO₄, and scan rate = 100 mV s⁻¹.

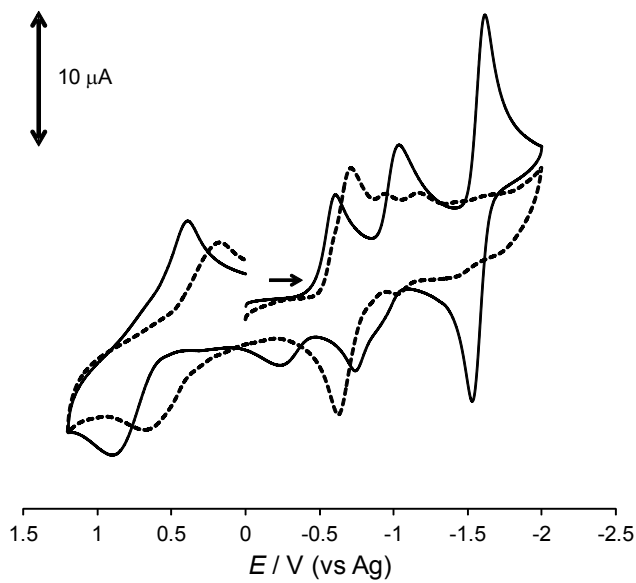


Figure S22. Cyclic voltammograms of complexes **1** and **2** in 2-butanone on a glassy carbon working electrode versus a Ag quasi-reference electrode. [complex **1**] = 1.02 mM (solid lines) and [complex **2**] = 1.08 mM (broken lines), supporting electrolyte = 0.10 M [$^n\text{Bu}_4\text{N}$] ClO_4 , and scan rate = 100 mV s $^{-1}$.

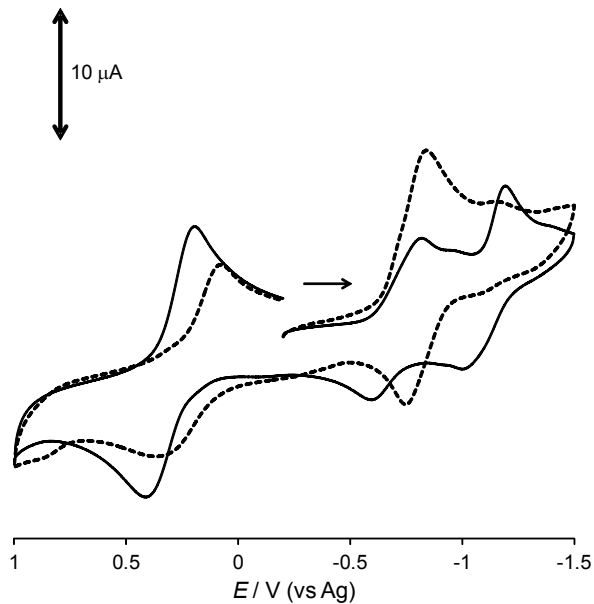


Figure S23. Cyclic voltammograms of complexes **1** and **2** in 1,2-difluorobenzene/acetone (4:1 v/v) on a glassy carbon working electrode versus a Ag quasi-reference electrode. [complex **1**] = 1.05 mM (solid lines) and [complex **2**] = 1.03 mM (broken lines), supporting electrolyte = 0.10 M [$^n\text{Bu}_4\text{N}$] ClO_4 , and scan rate = 100 mV s $^{-1}$.

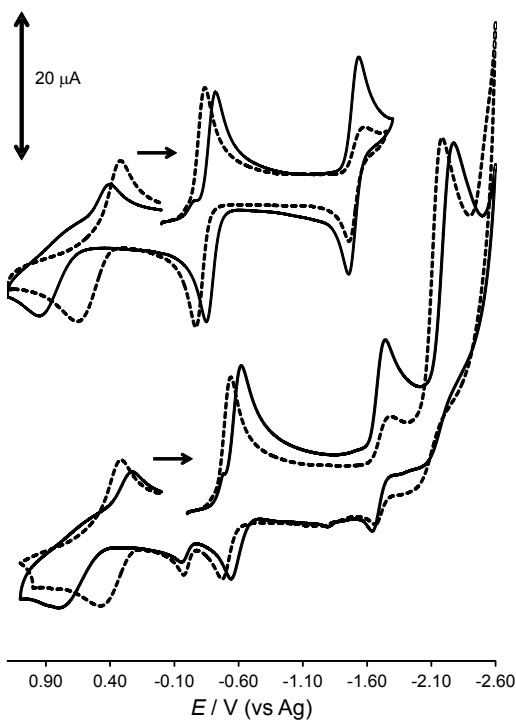


Figure S24. Cyclic voltammograms of complex **1** in CH_3CN on a glassy carbon working electrode versus a Ag quasi-reference electrode. [complex **1**] = 1.04 mM (solid lines) and [complex **1**] = 1.04 mM with 5.09 mM pyridine (broken lines), supporting electrolyte = 0.10 M [$^n\text{Bu}_4\text{N}\text{ClO}_4$, and scan rate = 100 mV s $^{-1}$.

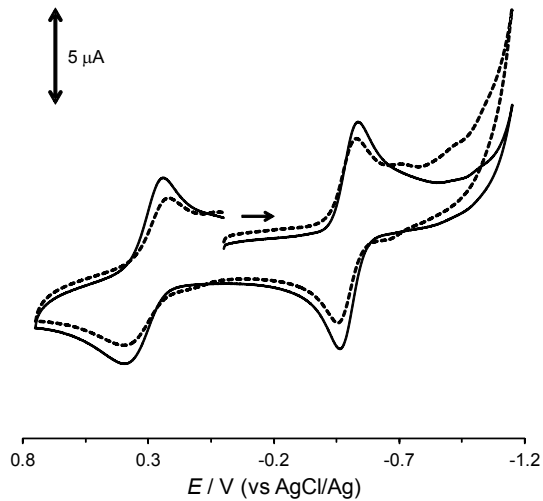


Figure S25. Cyclic voltammograms of complexes **1** and **2** in water with pyridine on a glassy carbon working electrode versus AgCl/Ag . [complex **1**] = 0.64 mM with 5.21 mM pyridine (solid lines) and [complex **2**] = 0.63 mM with 5.21 mM pyridine (broken lines), supporting electrolyte = 0.10 M NaClO_4 , and scan rate = 100 mV s $^{-1}$.

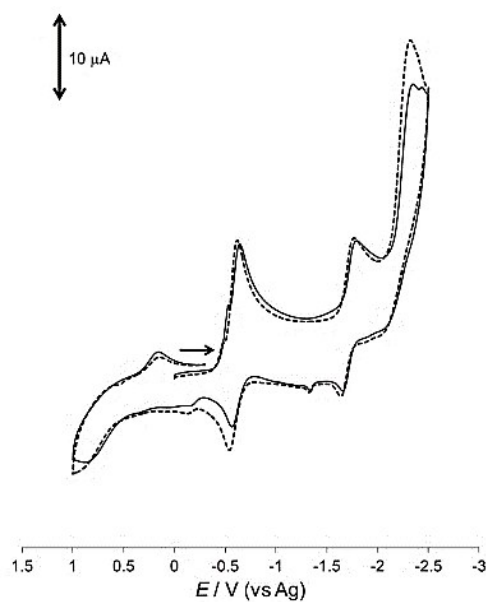


Figure S26. Cyclic voltammograms complex **1** in CH_3CN on a glassy carbon working electrode versus a Ag quasi-reference electrode. [complex **1**] = 1.02 mM (solid lines) and [complex **1**] = 1.02 mM with 15.0 mM 2-methylpyridine (broken lines), supporting electrolyte = 0.10 M [$^n\text{Bu}_4\text{N}$] ClO_4 , and scan rate = 100 mV s $^{-1}$.

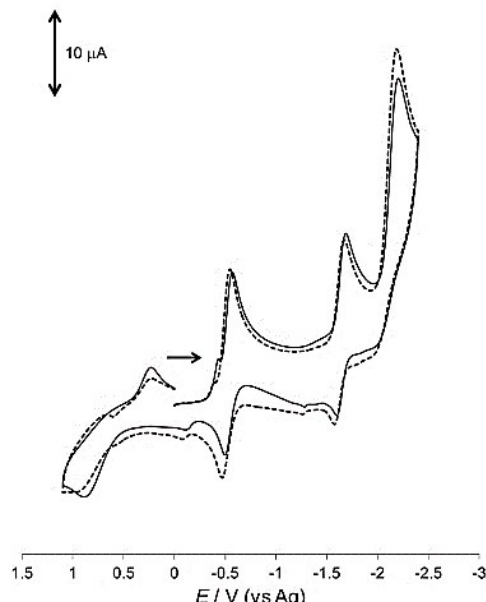


Figure S27. Cyclic voltammograms of complex **1** in CH_3CN on a glassy carbon working electrode versus a Ag quasi-reference electrode. [complex **1**] = 1.02 mM (solid lines) and [complex **1**] = 1.02 mM with 15.1 mM 2,6-dimethylpyridine (broken lines), supporting electrolyte = 0.10 M [$^n\text{Bu}_4\text{N}$] ClO_4 , and scan rate = 100 mV s $^{-1}$.

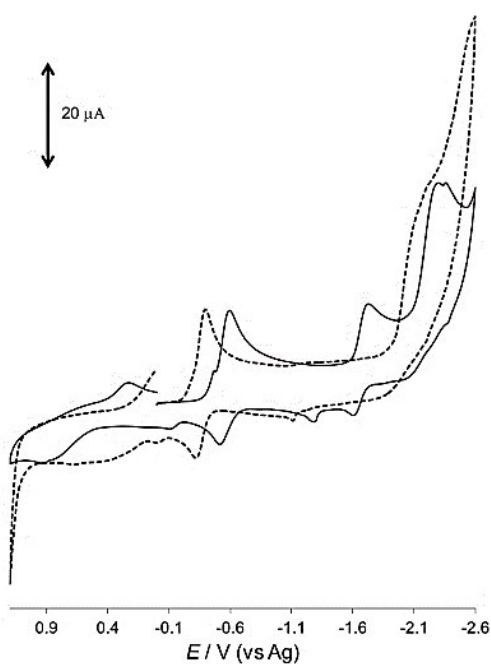


Figure S28. Cyclic voltammograms of complex **1** in acetonitrile on a glassy carbon working electrode versus a Ag quasi-reference electrode. [complex **1**] = 1.05 mM (solid lines) and [complex **1**] = 1.05 mM with [2-aminopyridine] = 5.10 mM (broken lines), supporting electrolyte = 0.10 M [ⁿBu₄N]ClO₄, and scan rate = 100 mV s⁻¹.

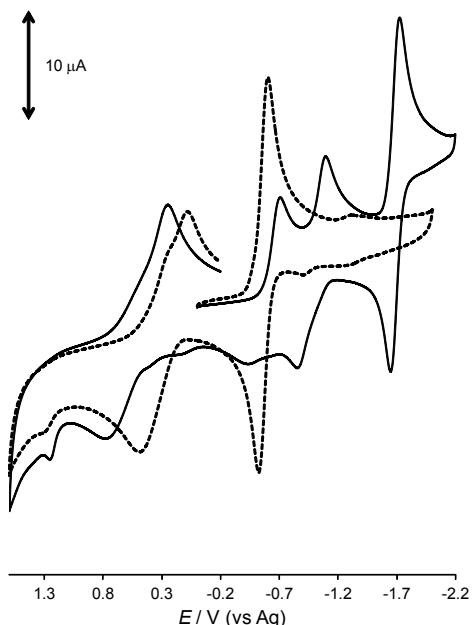


Figure S29. Cyclic voltammograms of complex **1** in acetone on a glassy carbon working electrode versus a Ag quasi-reference electrode. [complex **1**] = 1.04 mM (solid lines) and [complex **1**] = 1.04 mM with 5.09 mM of pyridine (broken lines), supporting electrolyte = 0.10 M [ⁿBu₄N]ClO₄, and scan rate = 100 mV s⁻¹.

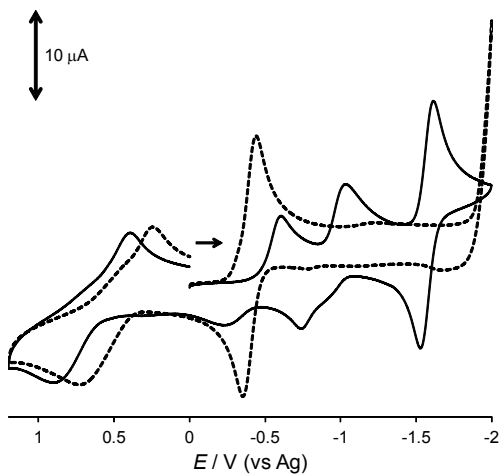


Figure S30. Cyclic voltammograms complex **1** in 2-butanone on a glassy carbon working electrode versus a Ag quasi-reference electrode. [complex **1**] = 1.02 mM (solid lines) and [complex **1**] = 1.02 mM with 5.09 mM of pyridine (broken lines), supporting electrolyte = 0.10 M [Bu_4N] ClO_4 , and scan rate = 100 mV s $^{-1}$.

1.4 Spectroelectrochemistry

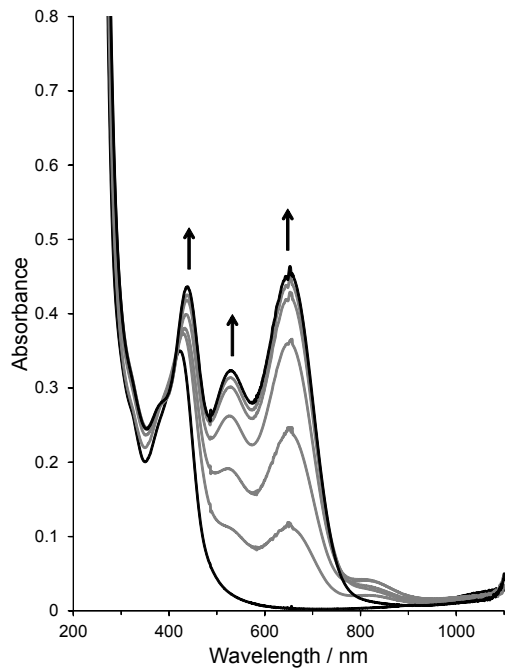


Figure S31. Absorbance changes in the UV-visible spectra of complex **1** with pyridine in acetonitrile at a constant potential of -1.0 V versus a Ag quasi-reference electrode. [complex **1**] = 1.05 mM, [pyridine] = 5.09 mM, supporting electrolyte = 0.10 M [Bu_4N] ClO_4 , and path length = 1 mm.

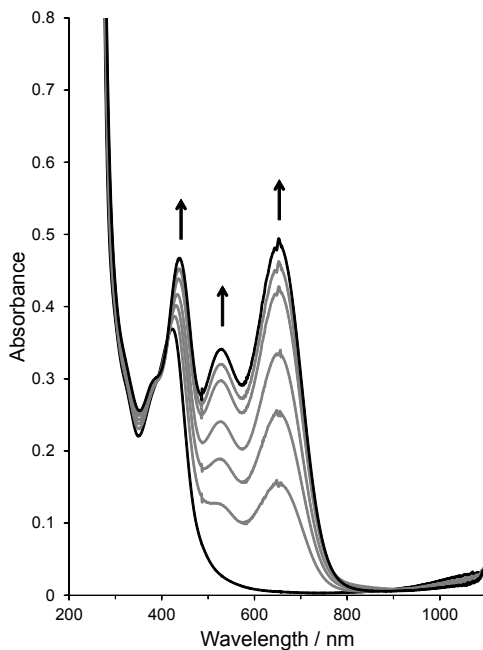


Figure S32. Absorbance changes in the UV-visible spectra of complex **1** with pyridine in acetonitrile at a constant potential of -1.0 V versus a Ag quasi-reference electrode. [complex **1**] = 1.05 mM, [pyridine] = 10.18 mM, supporting electrolyte = 0.10 M [$^{n}\text{Bu}_4\text{N}\text{ClO}_4$], and path length = 1 mm.

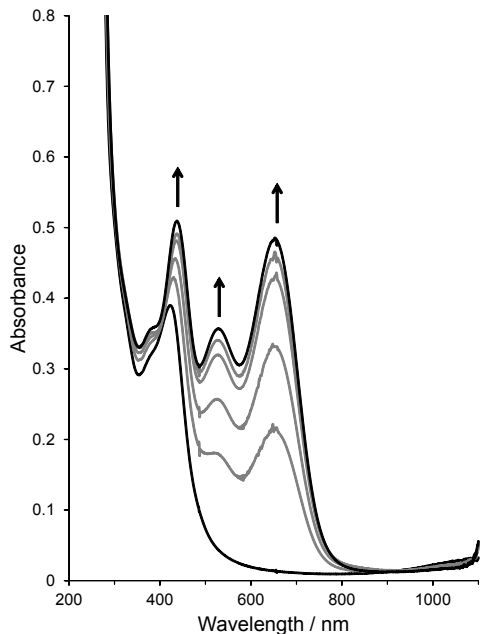


Figure S33. Absorbance changes in the UV-visible spectra of complex **2** with pyridine in acetonitrile at a constant potential of -1.0 V versus a Ag quasi-reference electrode. [complex **2**] = 1.02 mM, [pyridine] = 10.18 mM, supporting electrolyte = 0.10 M [$^{n}\text{Bu}_4\text{N}\text{ClO}_4$], and path length = 1 mm.

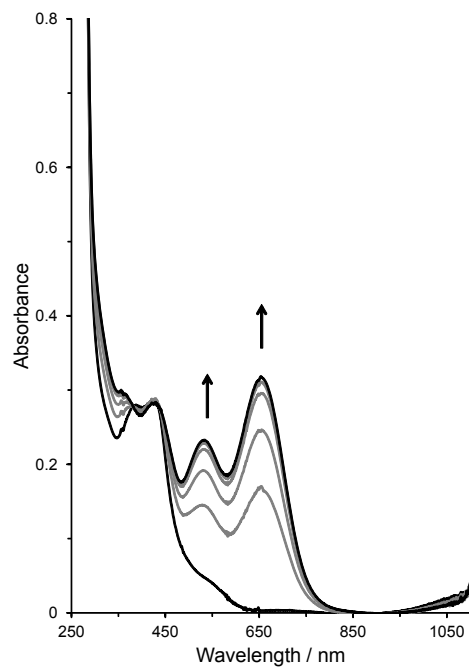


Figure S34. Absorbance changes in the UV-visible spectra of complex **1** with 2-aminopyridine in acetonitrile at a constant potential of -1.0 V versus a Ag quasi-reference electrode. [complex **1**] = 1.05 mM, [2-aminopyridine] = 5.10 mM, supporting electrolyte = 0.10 M [$^n\text{Bu}_4\text{N}$] ClO_4 , and path length = 1 mm.

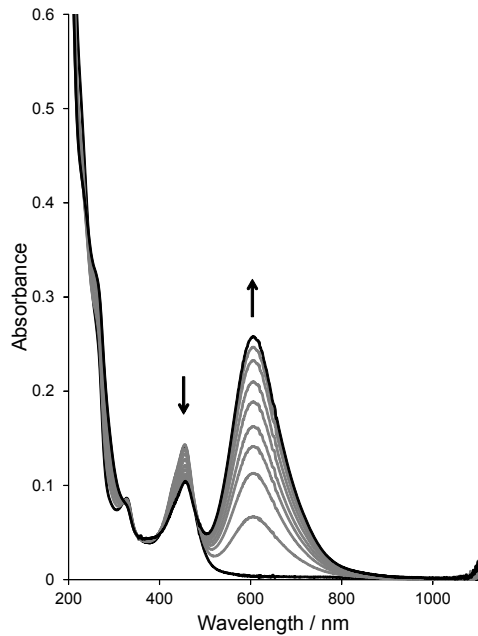


Figure S35. Absorbance changes in the UV-visible spectra of complex **1** in water at a constant potential of -0.75 V versus AgCl/Ag . [complex **1**] = 0.51 mM, supporting electrolyte = 0.10 M NaClO_4 , pH = 5.79, and path length = 1 mm. Note: At low pH (e.g., 2.30) the evolution of hydrogen is observed. The use of a buffer was avoided to eliminate substitution of the axial water ligands in complex **1** via anation.

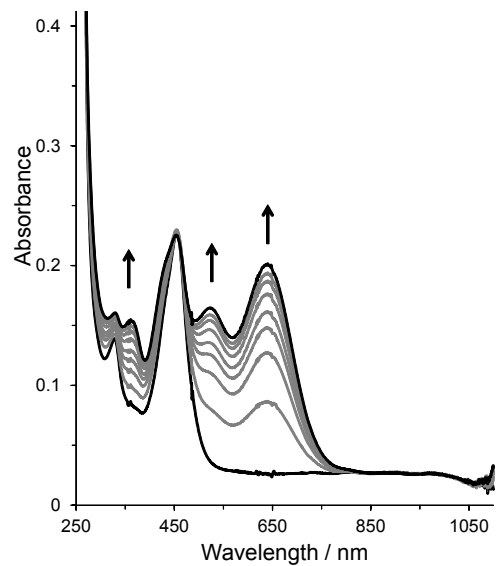


Figure S36. Absorbance changes in the UV-visible spectra of complex **1** in water at a constant potential of -0.70 V versus a Ag quasi-reference electrode. [complex **1**] = 0.60 mM, [pyridine] = 5.21 mM, supporting electrolyte = 0.10 M NaClO₄, pH = 4.58 , and path length = 1 mm.

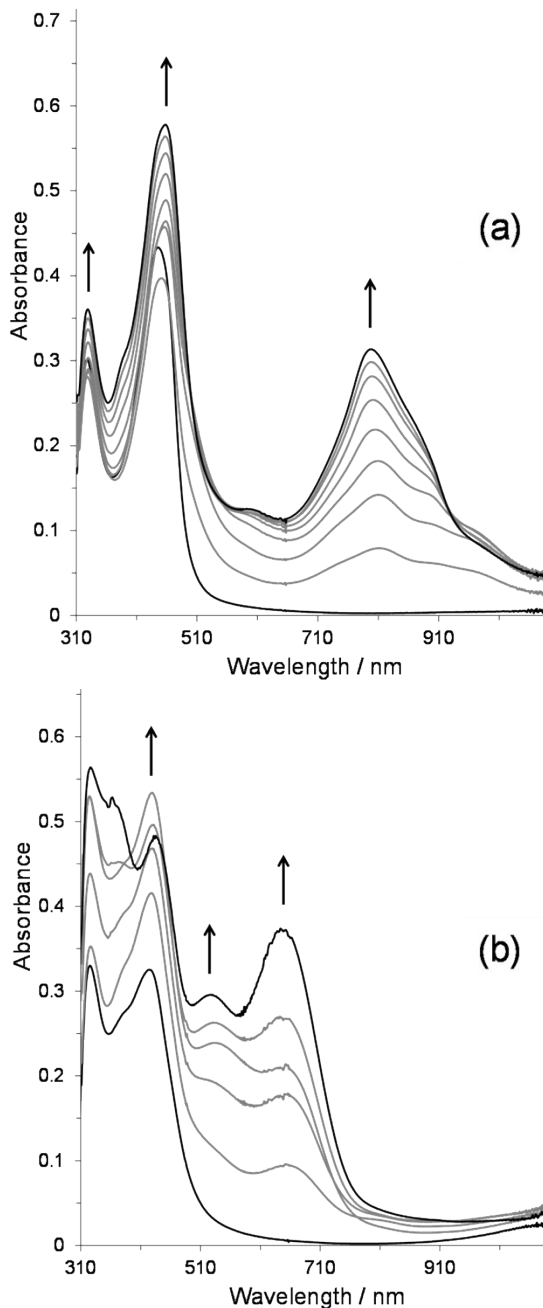


Figure S37. Absorbance changes in the UV-visible spectra of complexes **1** and **2** in acetone at a constant potential of -0.90 V versus a Ag quasi-reference electrode; supporting electrolyte = 0.10 M $[^n\text{Bu}_4\text{N}]\text{ClO}_4$, and path length = 1 mm. (a) [complex **1**] = 1.14 mM, (b) [complex **2**] = 1.08 mM.

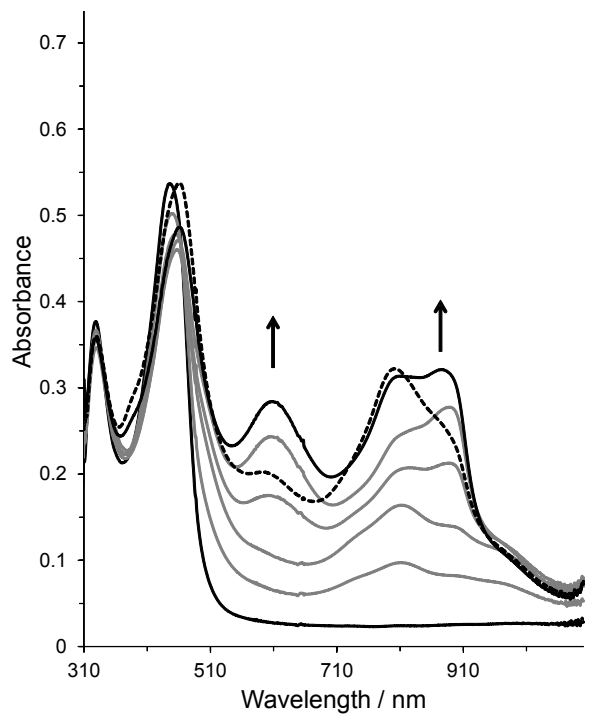


Figure S38. Absorbance changes in the UV-visible spectra of complex **1** in acetone at a constant potential of -1.30 V versus a Ag quasi-reference electrode. [complex **1**] = 1.14 mM, supporting electrolyte = 0.10 M [$^{n}\text{Bu}_4\text{N}^+$] ClO_4^- , and path length = 1 mm. Broken line illustrates the spectrum after an extended time.

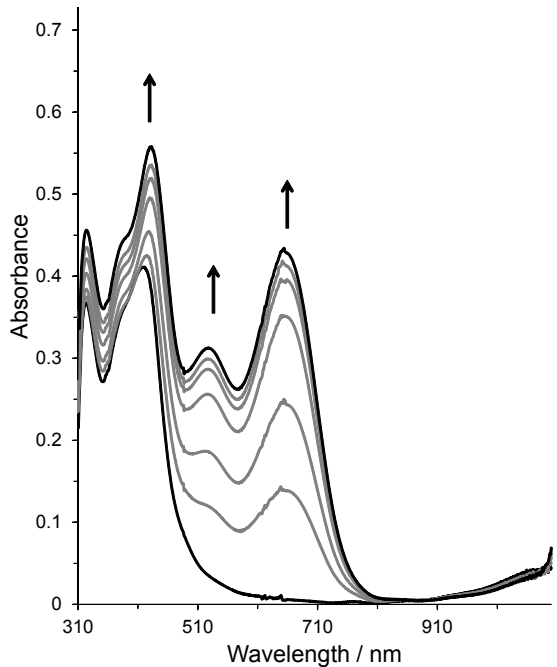


Figure S39. Absorbance changes in the UV-visible spectra of complex **1** with pyridine in acetone at a constant potential of -0.90 V versus a Ag quasi-reference electrode. [complex **1**] = 1.14 mM, [pyridine] = 5.09 mM, supporting electrolyte = 0.10 M [$^{n}\text{Bu}_4\text{N}^+$] ClO_4^- , and path length = 1 mm.

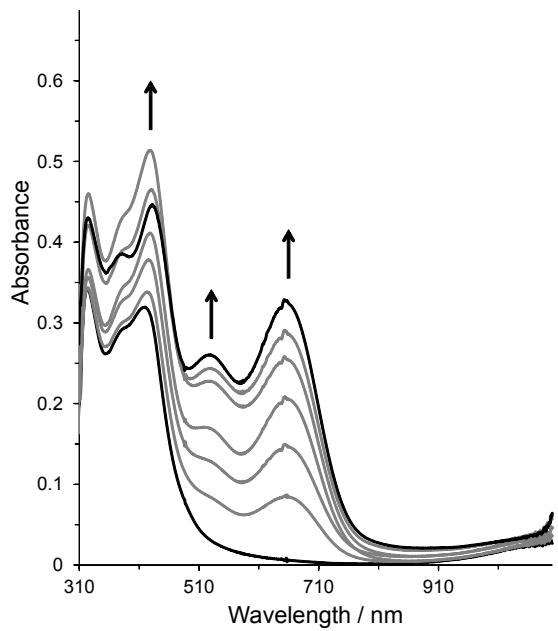


Figure S40. Absorbance changes in the UV-visible spectra of complex **2** with pyridine in acetone at a constant potential of -0.90 V versus a Ag quasi-reference electrode. [complex **2**] = 1.08 mM, [pyridine] = 5.09 mM, supporting electrolyte = 0.10 M [$^n\text{Bu}_4\text{N}\text{ClO}_4$], and path length = 1 mm.

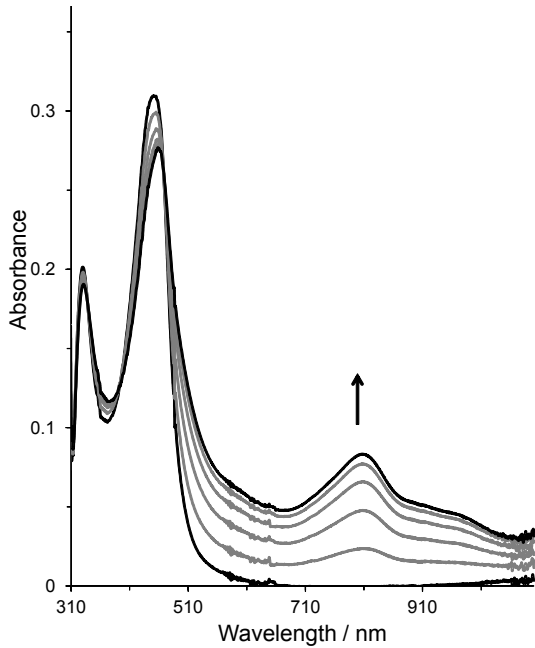


Figure S41. Absorbance changes in the UV-visible spectra of complex **1** in 2-butanone at a constant potential of -0.70 V versus a Ag quasi-reference electrode. [complex **1**] = 1.04 mM, supporting electrolyte = 0.10 M [$^n\text{Bu}_4\text{N}\text{ClO}_4$], and path length = 1 mm.

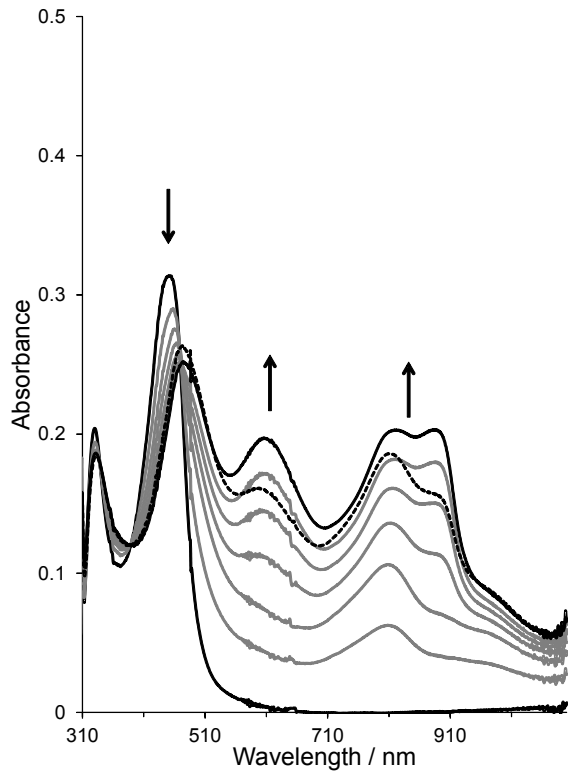


Figure S42. Absorbance changes in the UV-visible spectra of complex **1** in 2-butanone at a constant potential of -1.10 V versus a Ag quasi-reference electrode. [complex **1**] = 1.04 mM, supporting electrolyte = 0.10 M [$^n\text{Bu}_4\text{N}\text{ClO}_4$], and path length = 1 mm. Broken line illustrates the spectrum after an extended time.

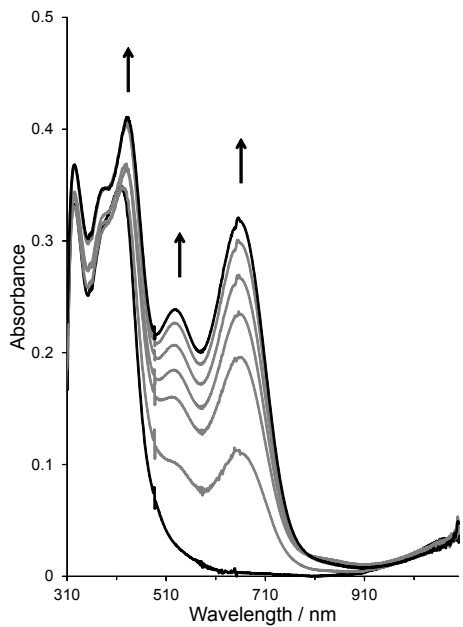


Figure S43. Absorbance changes in the UV-visible spectra of complex **1** with pyridine in 2-butanone at a constant potential of -0.70 V versus a Ag quasi-reference electrode. [complex **1**] = 1.04 mM, [pyridine] = 5.09 mM, supporting electrolyte = 0.10 M [$^n\text{Bu}_4\text{N}\text{ClO}_4$], and path length = 1 mm.

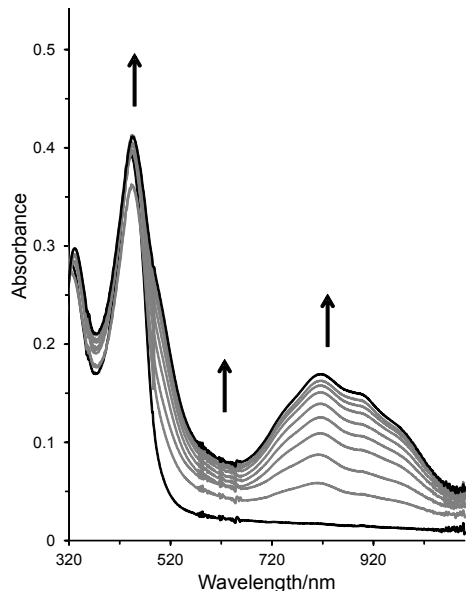


Figure S44. Absorbance changes in the UV-visible spectra of complex **1** in 1,2-difluorobenzene/acetone (4:1, v/v) at a constant potential of -0.90 V versus a Ag quasi-reference electrode. [complex **1**] = 1.05 mM, supporting electrolyte = 0.10 M [$^n\text{Bu}_4\text{N}\text{ClO}_4$], and path length = 1 mm.

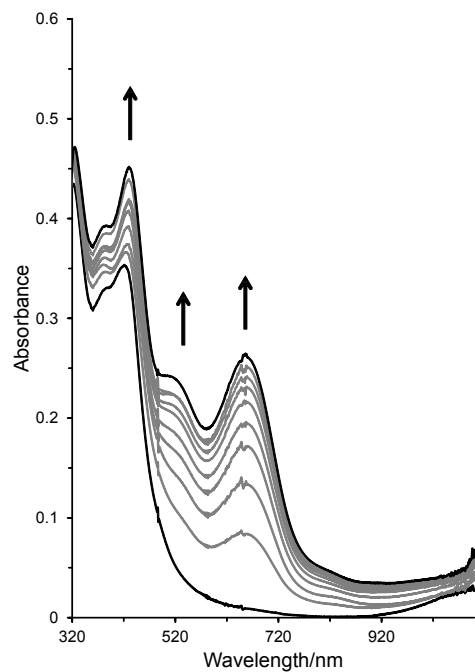


Figure S45. Absorbance changes in the UV-visible spectra of complex **2** in 1,2-difluorobenzene/acetone (4:1, v/v) at a constant potential of -0.90 V versus a Ag quasi-reference electrode. [complex **2**] = 1.03 mM, supporting electrolyte = 0.10 M [$^n\text{Bu}_4\text{N}\text{ClO}_4$], and path length = 1 mm.

1.5 ^{11}B , ^{19}F , and ^{59}Co NMR spectroscopic studies

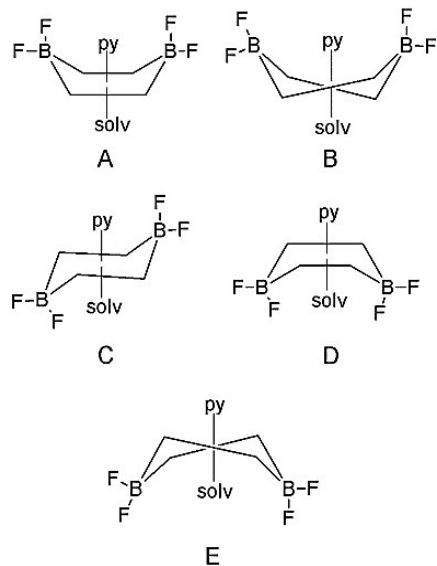


Figure S46. Conformers most likely adopted by the BF_2 caps of complex **2**.

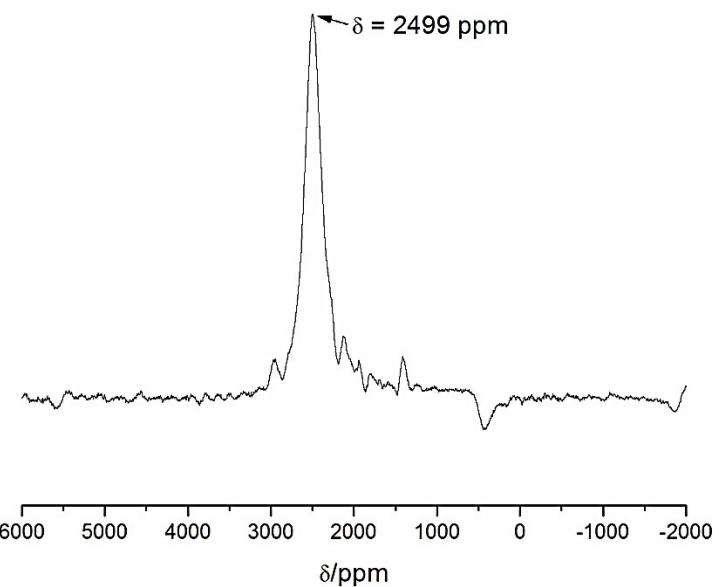


Figure S47. ^{59}Co NMR spectrum of the Co(I) species produced from 50 mM of complex **1**, 500 mM of $[^n\text{Bu}_4\text{N}]\text{BH}_4$, and 250 mM of 2,3,5,6-tetrafluoropyridine (pyF_4) in CD_3CN .

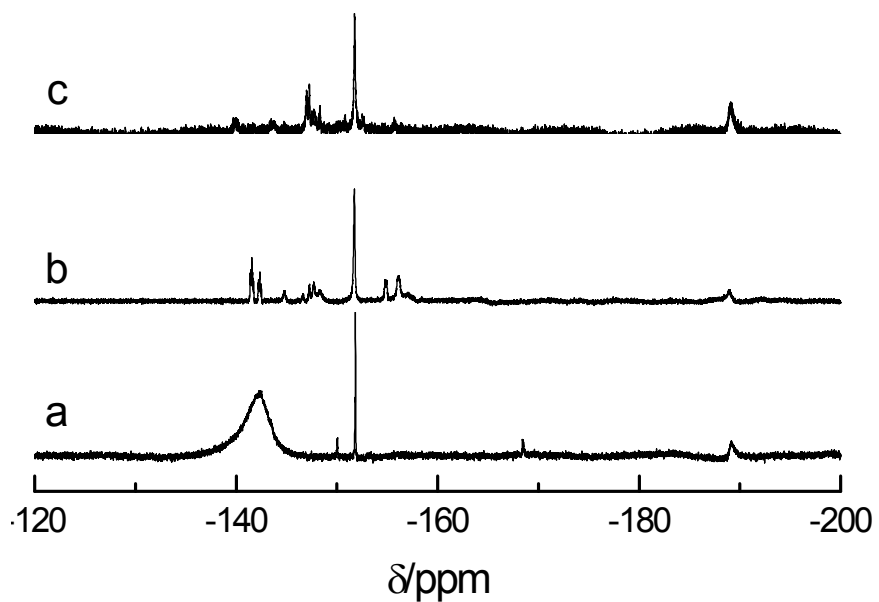


Figure S48. ^{19}F NMR spectra in CD_3CN of (a) 50 mM complex **1**, (b) 50 mM complex **2**, (c) 50 mM complex **1** with 250 mM pyridine.

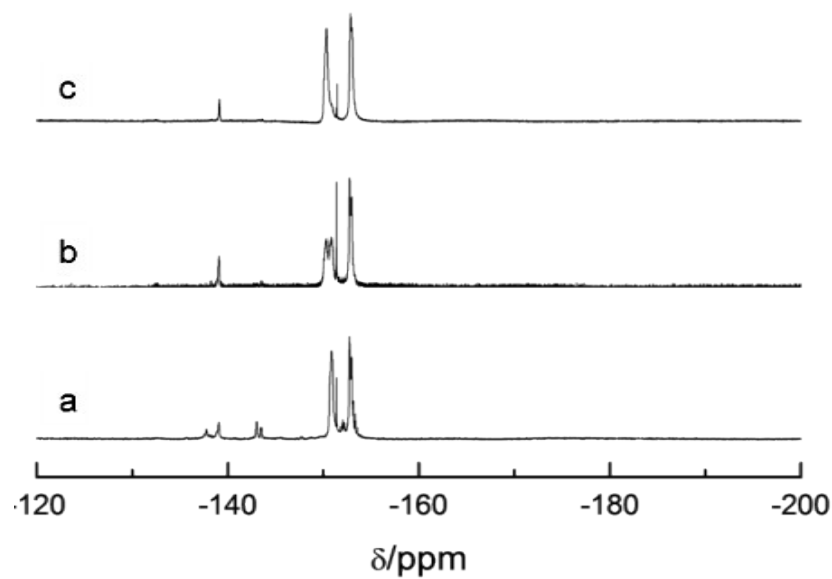


Figure S49. ¹⁹F NMR spectra acquired in CD₃CN of (a) 50 mM complex **1** with 500 mM [Bu₄N]BH₄; (b) 50 mM complex **2** with 500 mM [ⁿBu₄N]BH₄, and (c) 50 mM complex **1** with 250 mM pyridine and 500 mM [Bu₄N]BH₄.

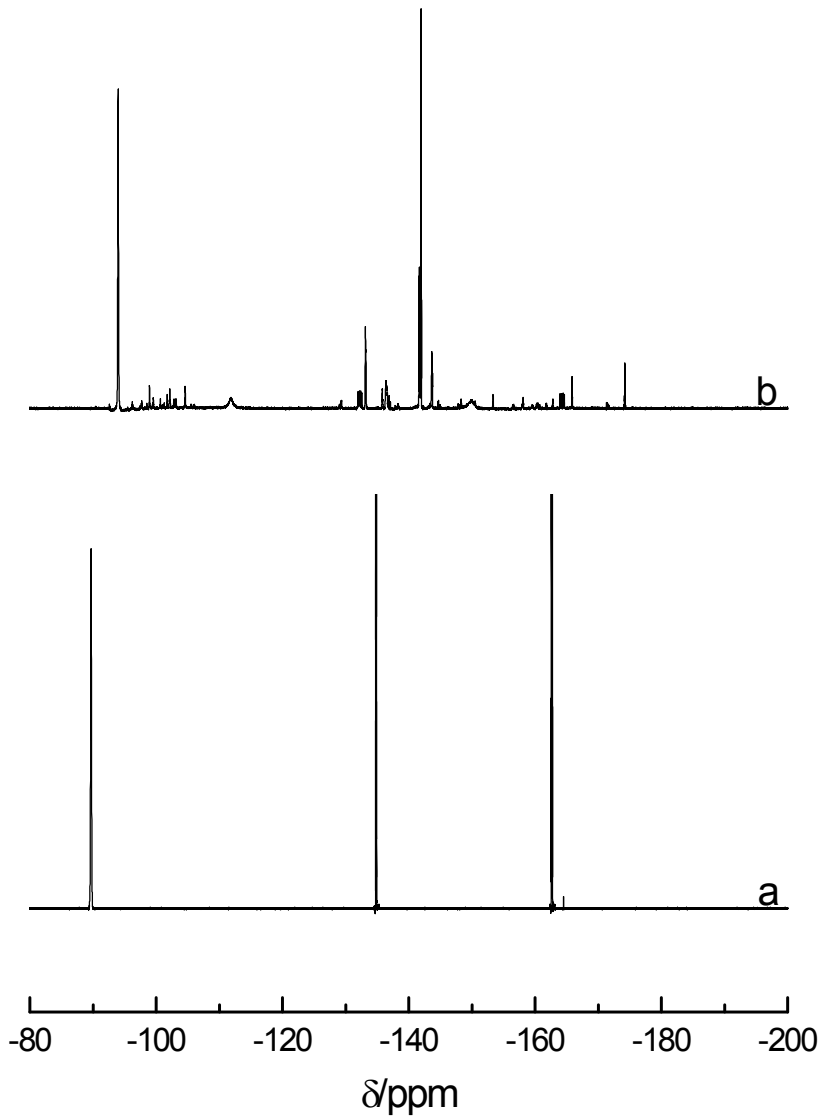


Figure S50. ¹⁹F NMR spectra in CD_3CN of (a) 250 mM pentafluoropyridine (pyF_5) and (b) 250 mM pyF_5 with 500 mM $[^n\text{BuN}]\text{BH}_4$.

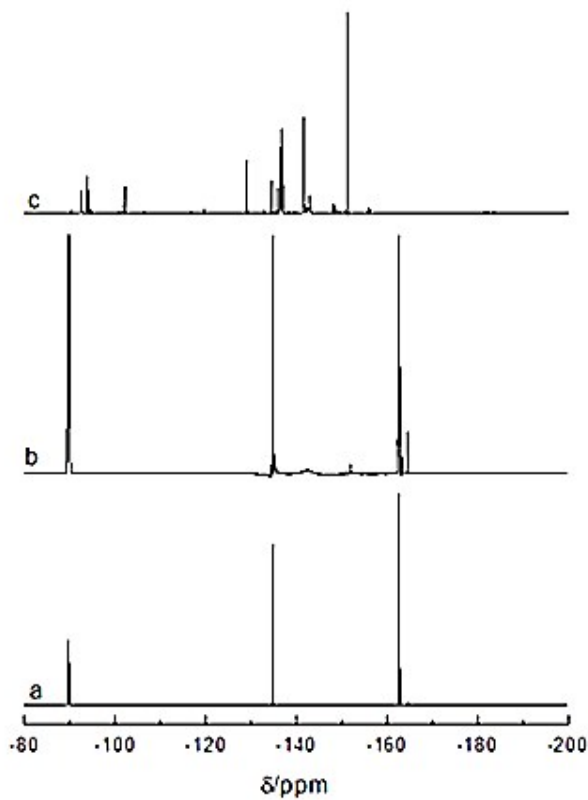
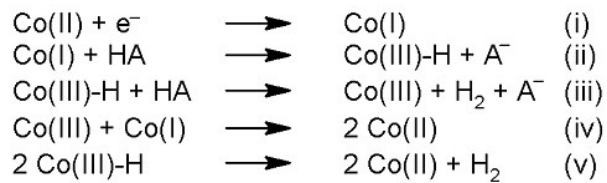


Figure S51. ^{19}F NMR spectra in CD_3CN for (a) 250 mM pyF_5 , (b) 50 mM complex **1** and 250 mM pyF_5 and (c) 50 mM complex **1**, 250 mM pyF_5 and 500 mM $[^n\text{Bu}_4\text{N}]BH_4$.

Table S7. ^{19}F and ^{11}B NMR chemical shifts for mixtures of $[\text{Co}(\text{dmgBF}_2)_2(\text{H}_2\text{O})_2]$ (complex **1**), fluorinated pyridines, and tetrabutylammonium tetrafluoroborate in CD_3CN .

| Entry | Species/mixture | δ_B / ppm | δ_F / ppm |
|-------|---|--|--|
| 1 | Complex 1 + $[^n\text{Bu}_4\text{N}]BH_4$ + pyF_5 | 19.63, 6.11 (t), 3.42, 3.26, 2.06, 1.51, 1.40, 0.95-0.45 (m) | -45.7, -48.4, -49.1, -69.3, -75.1, -89.6, -91.8, -93.2, -95.3, -96.3, -97.5, -98.8, -99.5, -99.9, -100.3, -101.3, -102.0, -103.8, -104.7, -105.4, -105.5, -108.7, -115.8, -118.9, -119.1, -119.9, -122.3, -128.2, -128.5, -130.6, -132.1, -136.0, -137.1, -138.7, -140.9, -141.1, -142.7, -147.4, -147.5, -147.5, -147.65, -147.7, -147.8, -150.6, -164.8, -173.5, |
| 2 | Complex 1 + $[^n\text{Bu}_4\text{N}]BH_4$ + pyF_4 | 19.92, 6.09, 3.44, 1.40, 0.79, -1.15, -10.60, -18.99, -19.69 | -48.8, -75.1, -89.6, -91.8, -93.2, -95.4, -95.8, -128.2, -128.5, -131.8, -135.0, -135.9, -136.1, -137.2, -138.2, -140.9, -141.1, -142.8, -147.4, -147.5, -147.5, -147.5, -150.1, -150.6, -150.6, -152.0, -152.2 |

1.6 Electrocatalytic behavior



Scheme S1. Proposed mechanism for the electrocatalytic reduction of protons (from an acid source, HA) by cobaloximes.¹

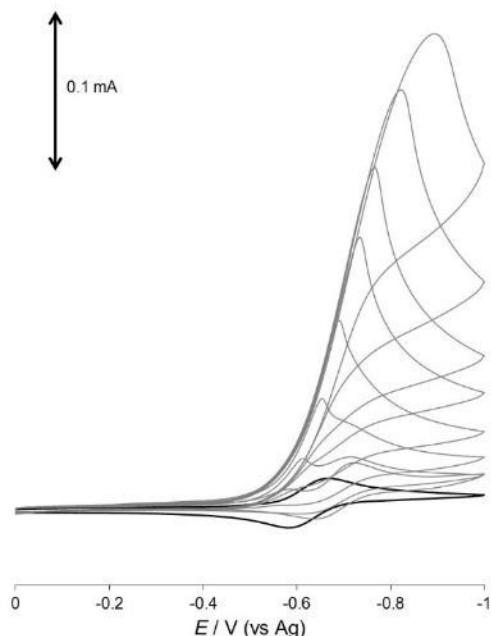


Figure S52. Cyclic voltammograms involving electrocatalysis with complex **2** in CH_3CN . [complex **2**] = 1.08 mM in the absence (black) and presence of aliquots of *p*-cyanoanilinium tetrafluoroborate (3.21, 5.54, 9.52, 13.8, 19.6, 25.3, 34.5, and 44.7 mM), supporting electrolyte = 0.10 M [$^n\text{Bu}_4\text{N}$] ClO_4 , and scan rate = 100 mV s⁻¹ at a glassy carbon working electrode versus a Ag quasi-reference electrode.

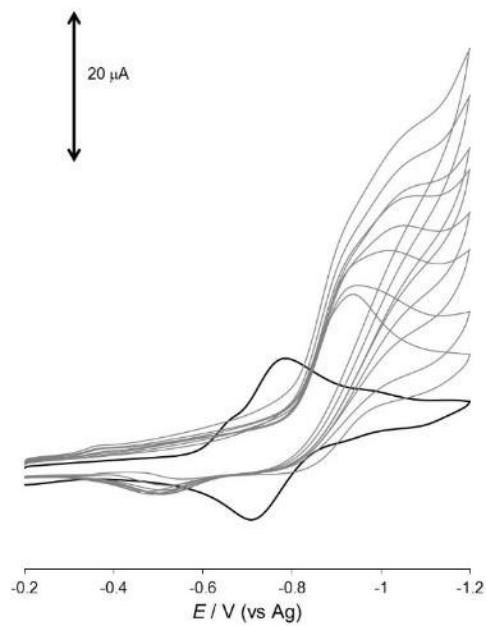


Figure S53. Cyclic voltammograms involving electrocatalysis with complex **1** in acetone. [complex **1**] = 1.08 mM in the absence (black) and presence of aliquots of *p*-cyanoanilinium tetrafluoroborate (1.80, 3.16, 4.52, 6.17, 8.74, 11.2, 14.9, and 18.6 mM), supporting electrolyte = 0.10 M [$^n\text{Bu}_4\text{N}\text{ClO}_4$, and scan rate = 100 mV s⁻¹ at a glassy carbon working electrode versus a Ag quasi-reference electrode.

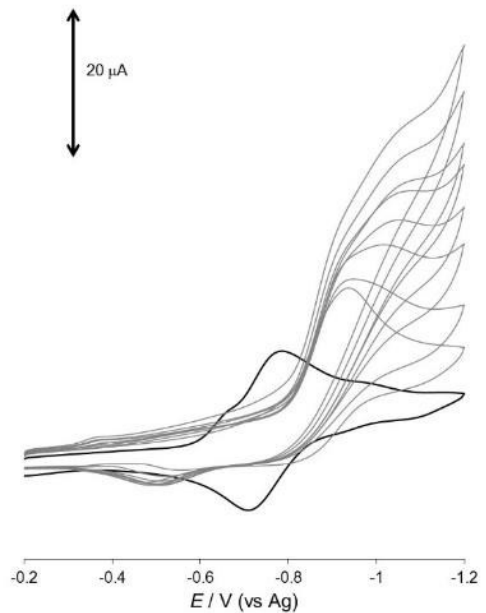


Figure S54. Cyclic voltammograms involving electrocatalysis with complex **2** in acetone. [complex **2**] = 1.08 mM in the absence (black) and presence of aliquots of *p*-cyanoanilinium tetrafluoroborate (1.70, 3.54, 5.24, 7.28, 9.42, 12.4, 16.1, and 18.7 mM), supporting electrolyte = 0.10 M [$^n\text{Bu}_4\text{N}\text{ClO}_4$, and scan rate = 100 mV s⁻¹ at a glassy carbon working electrode versus a Ag quasi-reference electrode.

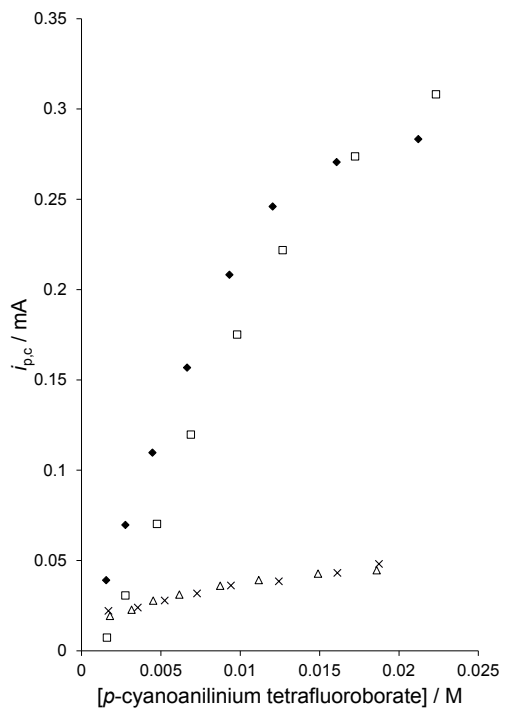


Figure S55. Dependence of the catalytic peak current ($i_{pc,l}$) on the concentration of *p*-cyanoanilinium tetrafluoroborate at a scan rate of 100 mV s⁻¹ for complex **1** (◆: in CH₃CN, Δ: in acetone) and complex **2** (□: in CH₃CN, ×: acetone) in 0.10 M [⁷Bu₄N]ClO₄, at a glassy carbon working electrode versus a Ag quasi-reference electrode.

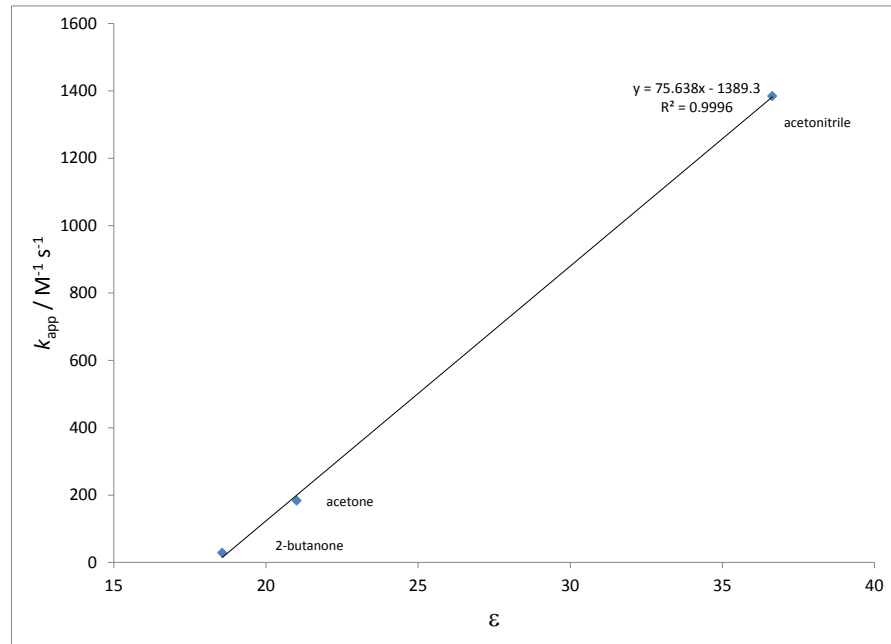


Figure S56. The effect of dielectric constant on k_{app} (from Table 6 of main text) for complex **1**.

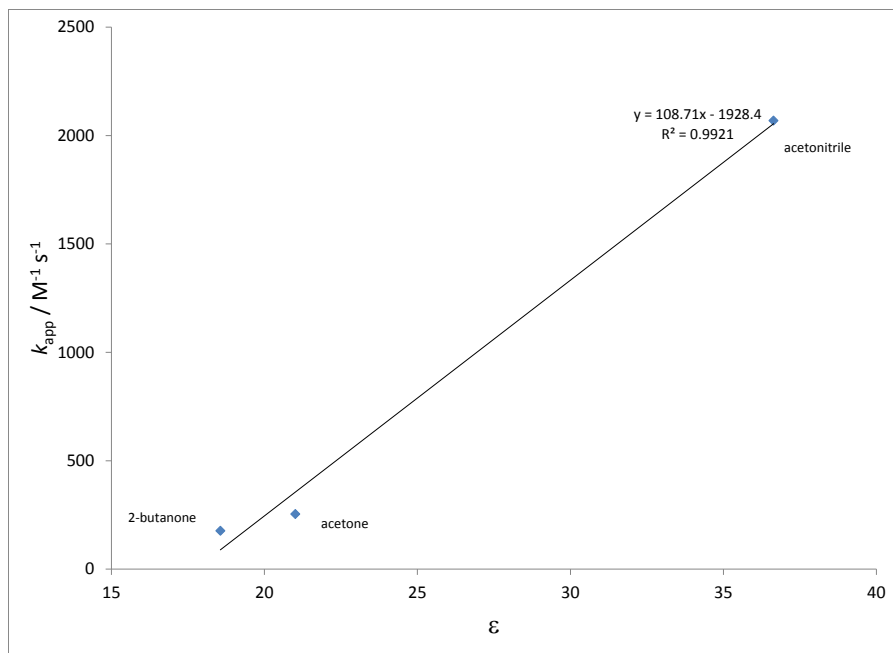


Figure S57. The effect of dielectric constant on k_{app} (from Table 6 of main text) for complex **2**.

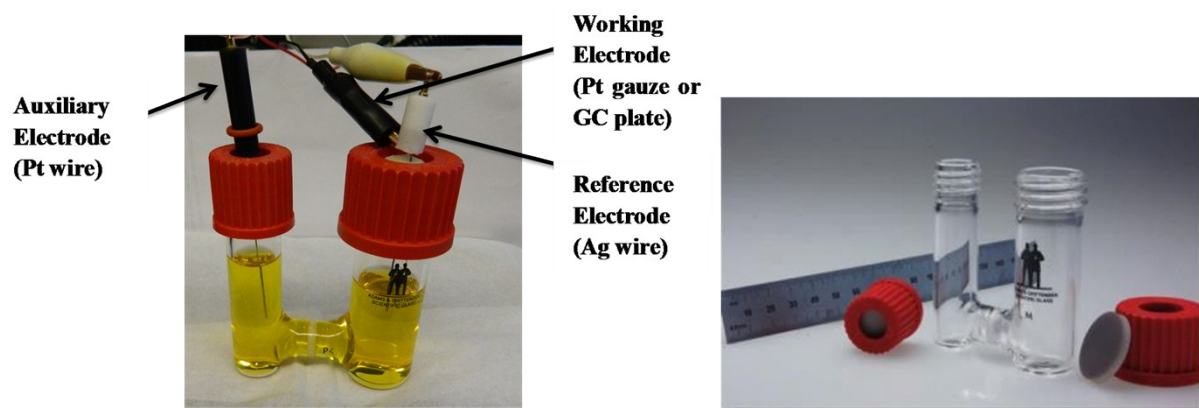


Figure S58. Setup of the H-Cell used for the electrocatalytic generation of hydrogen.

Reference

1. X. Hu, B. S. Brunschwig and J. C. Peters, *J. Am. Chem. Soc.*, 2007, **129**, 8988-8998.